doi:10.1017/S1431927622006985
Microsc. Microanal. 28 (Suppl 1), 2022

Direct Measurement of Atomic Reconstruction, Strain, and Disorder in Moiré Materials using 4D-STEM

Madeline Van Winkle[1], Nathanael P. Kazmierczak[1], Colin Ophus[2], Karen C. Bustillo[2], Stephen Carr[3], Hamish G. Brown[2], Jim Ciston[2] and D. Kwabena Bediako[1*]

[1.] Department of Chemistry, University of California, Berkeley, CA, United States.
[2.] National Center for Electron Microscopy, Molecular Foundry, Lawrence Berkeley National Laboratory, Berkeley, CA, United States.
[3.] Brown Theoretical Physics Center, Brown University, Providence, RI, United States.
* Corresponding author: bediako@berkeley.edu

Stacking two-dimensional van der Waals (vdW) bilayers with an offset in lattice periodicity— due to dissimilar lattice constants and/or rotational misalignment—produces a moiré superlattice with a periodicity that is inversely related to the magnitude of interlayer mismatch. The moiré pattern superimposes a nanoscale periodic potential on the vdW material and dramatically alters the electronic band structure of the system [1]. As such, moiré materials assembled from graphene, hexagonal boron nitride (hBN), and transition metal dichalcogenides (TMDs) have proven to be versatile platforms for designing electronic band structures [2-7]. For example, twisted bilayer graphene (TBG) displays a host of correlated electronic phases, including unconventional superconductivity [3] and ferromagnetism [4], as well as enhanced electrochemical activity [7] near an interlayer "magic angle" of 1.1°, which is associated with the formation of ultraflat electronic bands near the Fermi level.

While valued for their tunability, the unique band structures in moiré materials are fragile and can be easily manipulated by small structural deformations [8], disorder [9], and strain [10,11]. One of the most consequential structural modifications in moiré superlattices is an intrinsic lattice reconstruction process, which also generates intralayer strain and can suppress flat band formation in TBG [8]. In addition, extrinsic uniaxial heterostrain [10] and structural disorder, such as twist angle gradients [9], can both be introduced during the sample fabrication process. Visualizing the structure and strain fields of moiré superlattices is thus paramount to understanding and controlling their emergent electronic and chemical behavior.

Here, we demonstrate a technique based on four-dimensional scanning transmission electron microscopy (4D-STEM), termed Bragg interferometry (Fig. 1), that enables direct visualization of deformations underlying reconstruction, precise measurement of strain fields, and quantitative assessment of structural disorder in moiré superlattices (Fig. 2) [12]. TBG samples are fabricated using the 'tear-and-stack' method, introducing interlayer twist angles, θ_m, ranging from 0.1–1.6°. Four-dimensional STEM datasets are acquired using a Gatan K3 direct detection camera on a TEAM I microscope (aberration-corrected Thermo Fisher Scientific Titan 80–300) operated in energy-filtered STEM mode at 80 kV with a probe convergence angle of 1.71–3 mrad. There is interference between the electrons diffracted by the two layers of the moiré superlattice, leading to a modulation in the intensity of overlapping Bragg disks in the acquired diffraction patterns based on the local interlayer stacking order (Fig. 1a). Thus, a unique interlayer displacement vector can be calculated for each pixel in the 4D-STEM scans (Fig. 1b), yielding full displacement fields (Fig. 1c–e).

By differentiating the vector-valued displacement fields, we then probe the mechanics of lattice reconstruction at and near the magic angle in TBG (Fig. 2c), unveiling a previously undetected evolution of reconstruction as a function of twist angle that explains the frustration of flat band formation at theoretically predicted magic angles <1.1°. We also illustrate the strong interplay between reconstruction strain fields (Fig. 2d) and uniaxial heterostrain in TBG and evaluate intrinsic short-range disorder in the form of twist angle and heterostrain fluctuations (Fig. 2a, b). Our results provide a framework for directly visualizing structural relaxation, disorder, and strain in a wide array of moiré materials, including those in complex multilayer heterostructures [13].

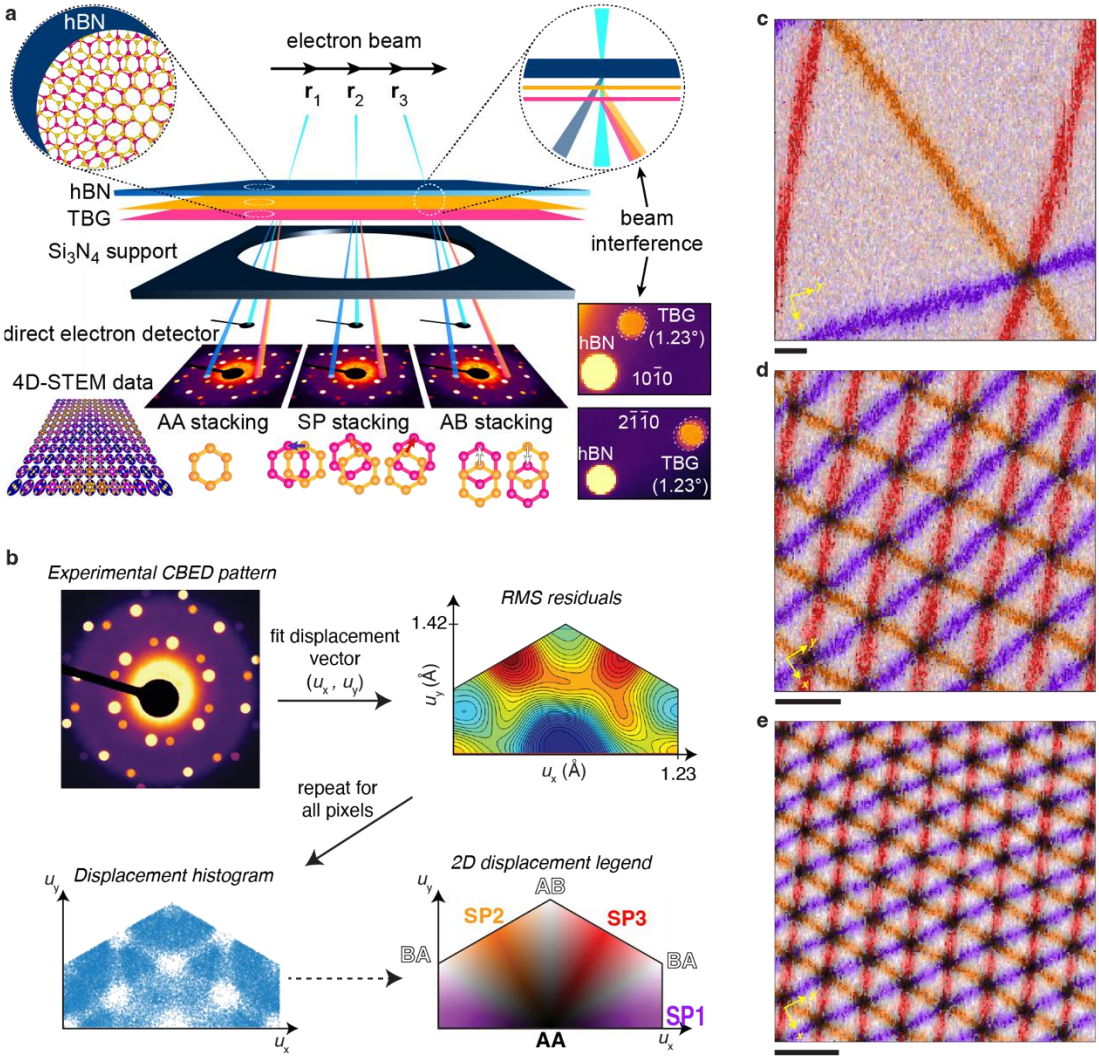

Figure 1. a) Schematic of 4D-STEM of an hBN/TBG heterostructure, showing Bragg disks of azimuthally misaligned layers. **b**) Schematic of the routine for fitting Bragg disk intensities to local displacement vectors **u**. The bottom-right image shows the 2D hue–value colorization scheme used to produce displacement maps from the fitted displacement vectors. **c–e**) Displacement field maps for TBG at with θ_m = 0.16° (**c**), 0.63° (**d**), and 1.03° (**e**). Scale bars 20 nm.

https://doi.org/10.1017/S1431927622006985 Published online by Cambridge University Press

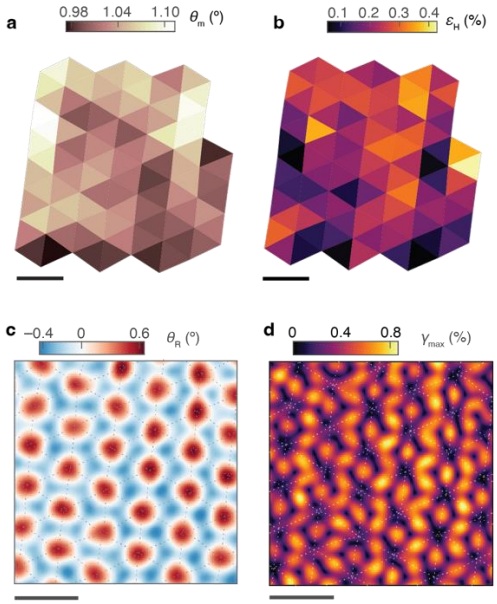

Figure 2. Maps showing intrinsic twist angle **(a)** and heterostrain **(b)** disorder, reconstruction rotation **(c)**, and maximum shear strain **(d)** generated from the displacement field in Fig. 1e, with an average θ_m = 1.03°. Scale bars 20 nm.

References:

[1] R. Bistritzer and A.H. MacDonald, Proc. Natl Acad. Sci. USA **108** (2011), p. 12233–12237.
[2] M. Yankowitz et al. Nat. Phys. **8** (2012), p. 382–386.
[3] Y. Cao et al. Nature **556** (2018), p. 43–50.
[4] A.L. Sharpe et al. Science **365** (2019), p. 605–608.
[5] C. Jin et al. Nature **567** (2019), 76–80.
[6] L. Wang et al. Nat. Mater. **19** (2020), 861–866.
[7] Y. Yu et al. Nat. Chem. (2022). doi: 10.1038/s41557-021-00865-1
[8] H. Yoo et al. Nat. Mater. **18** (2019), p. 448–453.
[9] A. Uri et al. Nature **81** (2020), p. 47–52.
[10] L. Huder et al. Phys. Rev. Lett. **120** (2018), 156405.
[11] Z. Bi, N.F.Q. Yuan, and L. Fu, Phys. Rev. B **100** (2019), 035448.
[12] N.P. Kazmierczak et al. Nat. Mater. **20** (2021), 956–963.
[13] Major experimental work supported by the Office of Naval Research Young Investigator Program under award no. N00014-19-1-2199 (D.K.B.). M.V.W. acknowledges support from an NSF GRFP award and a UC Berkeley Chancellor's Fellowship. Work at the Molecular Foundry was supported by the Office of Science, Office of Basic Energy Sciences, of the US Department of Energy under contract no. DE-AC02-05CH1123. C.O. acknowledges the support of the Department of Energy Early Career Research Award program. S.C. acknowledges support from the NSF through grant no. OIA-1921199. J.C. and H.G.B. acknowledge support from the Presidential Early Career Award for Scientists and Engineers (PECASE) through the US Department of Energy. D.K.B. acknowledges support from the Rose Hills Foundation through the Rose Hills Innovator Program.